

Triple-Pnictogen Bonding as a Tool for Supramolecular Assembly

Shiva Moaven,[†] Miranda C. Andrews,^{†,ID} Thomas J. Polaske,[‡] Brian M. Karl,[‡] Daniel K. Unruh,^{†,ID} Eric Bosch,^{§,ID} Nathan P. Bowling,^{*,‡,ID} and Anthony F. Cozzolino^{*,†,ID}

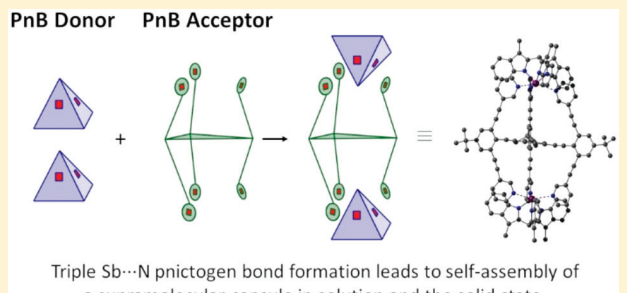
[†]Department of Chemistry and Biochemistry, Texas Tech University, 1204 Boston Avenue, Lubbock, Texas 79409-1061, United States

[‡]Department of Chemistry, University of Wisconsin—Stevens Point, 2101 Fourth Avenue, Stevens Point, Wisconsin 54481, United States

[§]Chemistry Department, Missouri State University, 901 S. National Ave., Springfield, Missouri 65897, United States

Supporting Information

ABSTRACT: Supramolecular assembly utilizing simultaneous formation of three pnictogen bonds around a single antimony vertex was explored via X-ray crystallography, solution NMR, and computational chemistry. An arylethynyl (AE) ligand was designed to complement the three electrophilic regions around the Sb compound. Though solution studies reveal large binding constants for individual pyridyl units with the Sb donor, the rigidity and rearrangement of the AE acceptor proved necessary to achieve simultaneous binding of three acceptors to the Sb-centered pnictogen-bond donor. Calculations and X-ray structures suggest that negative cooperativity upon sequential binding of three acceptors to a Sb center limits the utility of triple-pnictogen bonding pyridyl acceptors. These limitations can be negated, however, when positive cooperativity is designed into a complementary acceptor ligand.



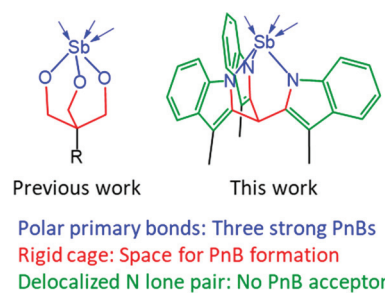
chalcogen-bond donors, heavier pnictogen atoms such as Sb and Bi can also behave as electrophiles and form strong pnictogen bonds (PnB). Covalently bound trivalent pnictogen atoms offer the possibility of three localized σ -holes and, therefore, the potential for triple pnictogen bonding at a single pnictogen (Scheme 1).^{23,24} This has been nicely demonstrated

INTRODUCTION

Multivalent interactions are often necessary in the design of complex and robust supramolecular assemblies. For instance, halogen and chalcogen bonding can be used in the construction of supramolecular capsules when multiple halogen or chalcogen binding sites are installed on a molecular cavitand.^{1–3} Halogen and chalcogen bonding are examples of secondary bonding or σ -hole interactions in which the attraction of a nucleophilic region on one molecule toward an electrophilic region on a halogen or chalcogen atom in another is exploited.^{4–8} The strength of σ -hole attractions is correlated with the size of the atom acting as the donor ($I > Br > Cl \gg F$ and $Te > Se > S \gg O$) and the extent to which electron withdrawing substituents accentuate the electrophilic regions.^{9,10} These regions are found along the extension of covalent bonds so that a halogen possesses a single σ -hole approximately 180° across from the covalent bond and a typical chalcogen possesses two σ -holes approximately 180° from each covalent bond.

Lewis acidic antimony(V) compounds have led to exciting advances in anion recognition and sensing,^{11–14} anion transport,¹⁵ and catalysis.^{16–19} Trivalent pnictogen atoms possess a lone pair, and their compounds often serve as Lewis bases, particularly with the lighter pnictogens. To this end, phosphine compounds are often employed as ligands supporting organometallic compounds and catalysts,²⁰ and the triphenyl compounds, PPh_3 , AsPh_3 , and SbPh_3 , have been used as halogen bond acceptors.^{21,22} Similar to strong halogen- and

Scheme 1. Triple PnB Donors



through cocrystallization of antimony halides with crown (thio)ethers.^{23–29} Few examples exist of the purposeful use of this unique spatial arrangement of three σ -holes for supramolecular chemistry to date.^{24,30–32} One can imagine forming assemblies via simultaneous binding of three Lewis basic electron donors (PnB acceptors), with the pnictogen atom

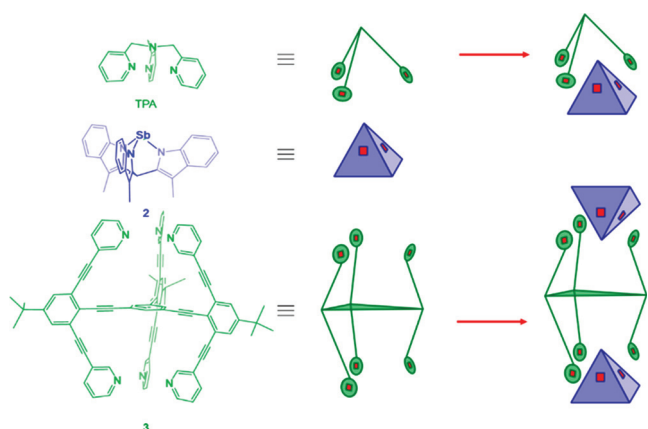
Received: September 17, 2019

Published: November 13, 2019

serving as a trigonal vertex of a polygon. To achieve this, a cage-structure that allows sufficient space around the pnictogen atom to form three primary and three secondary bonds is necessary. A cage that has previously proved able to facilitate self-assembly through multiple PnBs^{24,30} has been adapted for this study (Scheme 1). Strong PnBs are facilitated by polar primary bonds. In the case of Pn–O bonds, the formation of strong interactions has been demonstrated but the molecules are ambiphilic, where they act simultaneously as the PnB donor and acceptor.^{24,30,33,34} One approach to prevent self-recognition is to utilize perfluorinated alkyl/aryl groups. Matile et al. demonstrated that the PnB formed with tris-(perfluorophenyl)stibene can be quite strong (the V_{\max} on the ESP surface is 172 kJ/mol) but only one such V_{\max} was accessible on the molecular surface.²³ To achieve a triple PnB donor that does not undergo self-recognition, the approach used here is to support the pnictogen with nitrogen in the primary bonds to retain bond polarity. Incorporation of the nitrogen into an indole ring delocalizes the N-lone pair, reducing its efficiency as a pnictogen bond acceptor. Finally, incorporating the pnictogen into a cage ensures sufficient space at the pnictogen for the formation of up to three PnBs (Scheme 1).

A supramolecular building block that is complementary to a triple PnB donor (Scheme 1) must include three lone-pairs in an arrangement that allows for alignment with the electrophilic regions. Beyond that, building blocks for a functional PnB-based supramolecular cavitand should contain both spacers that create an internal cavity and some level of preorganization favoring simultaneous PnB of three acceptor units. Polypyridyl-containing molecules have previously been employed as chelating ligands in coordination chemistry and as halogen and hydrogen bond acceptors in supramolecular design.^{1,35–39} Arylene ethynylene (AE) 3 has been designed in this study to provide a rigid template that allows the three pyridine acceptors on each side an equatorial plane to form simultaneous PnB interactions, creating small cavities above and below the central 1,3,5-substituted benzene core of the complex (Scheme 2). The different binding behavior of ligand 2 versus the flexible tris(2-pyridylmethyl)amine (TPA) systems is rationalized by studying binding of the PnB donor with not only these threefold acceptors but also monodentate PnB acceptors in the solid state, in solution, and computationally in the gas phase.

Scheme 2. Design of a Triple PnB Donor



RESULTS AND DISCUSSION

Computational Evaluation of Triple Pnictogen Bond Donor. Density functional theory (DFT) calculations (B97-D3, ZORA, def2-TZVPP) were used to evaluate the ability of **2** to form pnictogen bonds. The geometry was optimized starting from the crystallographic coordinates. No significant deviation from the experimental geometry was noted. The Fukui function ($f^*(r)$) integrated from above and the electrostatic potential energy (ESP) were separately mapped onto the molecular surface as represented by the 0.001 au isosurface of the electron density of **2** (Figure 1). The Fukui function

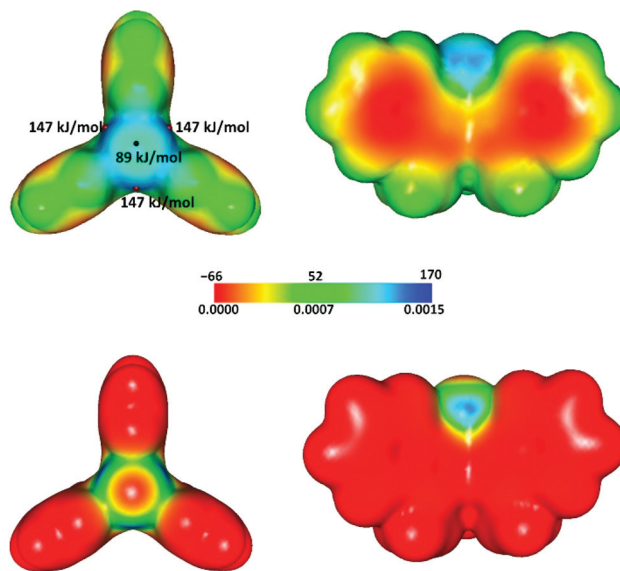


Figure 1. Electrostatic potential (top) and Fukui function (bottom) of **2** from two different views mapped on the electron density surface (0.001 au isosurface). The red and black spheres indicated on the ESP are V_{\max} and V_{\min} positions, respectively. ESP units are in kJ/mol.

depicts electrophilic regions according to an orbital model. The ESP map depicts three regions of high electrostatic potential (V_{\max}) that coincide with the electrophilic regions depicted by the Fukui function. Each of the three V_{\max} values of 147 kJ/mol are on par with the values reported on the 0.001 au molecular surface for neutral systems that engage in strong halogen,^{23,40} and chalcogen^{23,41} bonds. The presence of these three well-resolved sites is a strong indicator of the ability of **2** to form multiple predictable PnBs.

Preparation and Characterization of Triple Pnictogen Bond Donor

Treatment of tris-indole **1**⁴² with antimony(III) diethylamide in anhydrous benzene gives the desired compound, **2**, in high yield (see Scheme 3). The clean loss of the indole NH peak was observed by ¹H NMR and IR spectroscopies.

Yellow hexagonal single crystals of **2** were grown directly from a solution of **1** and $\text{Sb}(\text{NEt}_2)_3$ upon sitting in anhydrous benzene at room temperature. The crystal structure (Figure 2) reveals a molecule of **2** without any pnictogen bonds. Due to the high molecular symmetry, all the Sb–N bonds are equivalent with a length of 2.057(3) Å. A benzene ring is sandwiched between two staggered molecules of **2** with an Sb– C_6H_6 (centroid) distance of 3.648 Å, longer and at a different angle than typically observed for Menshutkin complexes,^{43–45}

Scheme 3. Synthesis of 2

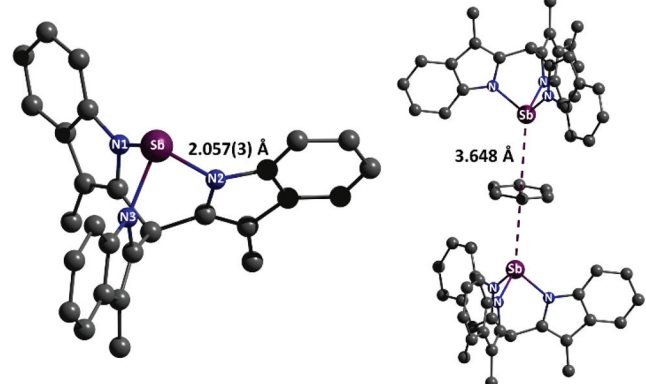
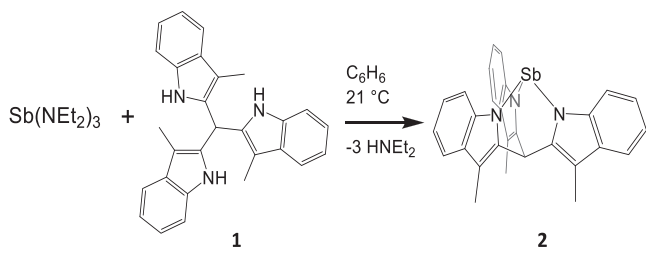


Figure 2. Ball and stick representation of crystal structure of $2\text{-C}_6\text{H}_6$ showing only 2 (left) and the arrangement of benzene between two molecules of 2 (right). Hydrogen atoms are omitted for clarity.

suggesting that the benzene facilitates packing rather than forming strongly attractive interactions with the antimony.

The powder X-ray diffraction pattern of the dried bulk powder matches the simulated pattern of $2\text{-C}_6\text{H}_6$ from the single crystals (Figure S34); however, the ^1H NMR spectrum of the material reveals only half an equivalent of benzene (Figure S14) which appears as free benzene according to the unperturbed chemical shifts. Presumably, the interstitial benzene has been lost from the lattice during drying. This is consistent with a formula of $2\text{-1/2C}_6\text{H}_6$ which matches the results of elemental analysis.

Self-Assembly through Triple Pnictogen Bonds. Preliminary DFT calculations (B97-D3, ZORA, def2-TZVPP) suggested that tridentate TPA would bind with the formation of three equivalent PnBs as depicted in Scheme 2. Treatment of 2 with an equimolar amount of TPA in toluene yielded single crystals of 2-TPA. Contrary to the DFT minimized structure, the crystal structure of 2-TPA revealed that self-assembly occurred via the formation of two PnBs (Figure 3). The Sb interacts with N_5 and N_6 at distances of $2.754(2)$ Å (76% of Σr_{vdW} or 131% of Σr_{cov}) and $2.615(2)$ Å (72% of Σr_{vdW} or 124% of Σr_{cov}), respectively.^{46,47} The Sb–N primary bonds are, on average, 1.77% elongated as compared to those in the structure of $2\text{-C}_6\text{H}_6$ (see Table 1). This can be rationalized, according to an orbital model, by considering the PnB being stabilized by the overlap of the N-lone pairs with the Sb–N σ^* orbitals. There is another close contact between Sb and N_4 with a distance of $3.330(2)$ Å (92% of Σr_{vdW} or 159% of Σr_{cov}). An AIM (atoms in molecules) analysis (see Table 2) reveals a low density at the bond critical point (bcp), consistent with the short distance being geometrically enforced, rather than the result of a favorable interaction. The third pyridyl group did not form a PnB with the third electrophilic region on the antimony atom in 2-TPA.

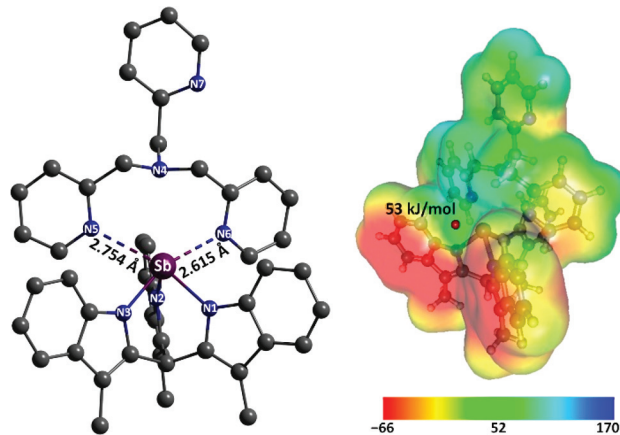


Figure 3. (Left) Ball and stick representation of crystal structure of 2-TPA (hydrogens were omitted for clarity). (Right) Electrostatic potential of 2-TPA on 0.001 au electron density of supramolecule (red sphere indicated on the ESP represents $V_{\text{S},\text{max}}$). ESP units are in kJ/mol.

Table 1. Selected Crystallographic Bond Distances (Å)

compd	$\text{Sb}-\text{N}_n$	$\text{Sb}\cdots\text{N}_n$
2	$\text{Sb}-\text{N}_1$ 2.057(3)	
	$\text{Sb}-\text{N}_2$ 2.057(3)	
	$\text{Sb}-\text{N}_3$ 2.057(3)	
2-Py_2	$\text{Sb}-\text{N}_1$ 2.037(5)	$\text{Sb}\cdots\text{N}_4$ 2.716(6)
	$\text{Sb}-\text{N}_2$ 2.074(13)	$\text{Sb}\cdots\text{N}_5$ 2.716(6)
	$\text{Sb}-\text{N}_3$ 2.037(5)	
2-BP	$\text{Sb}-\text{N}_1$ 2.074(2)	$\text{Sb}\cdots\text{N}_4$ 2.637(2)
	$\text{Sb}-\text{N}_2$ 2.098(2)	$\text{Sb}\cdots\text{N}_5$ 3.197(2)
	$\text{Sb}-\text{N}_3$ 2.0647(2)	
2-TPA	$\text{Sb}-\text{N}_1$ 2.092(2)	$\text{Sb}\cdots\text{N}_4$ 3.330(2)
	$\text{Sb}-\text{N}_2$ 2.070(2)	$\text{Sb}\cdots\text{N}_5$ 2.754(2)
	$\text{Sb}-\text{N}_3$ 2.118(2)	$\text{Sb}\cdots\text{N}_6$ 2.615(2)
$\alpha-2_2\cdot 3$	Sb_1-N_1 2.108(4)	$\text{Sb}_1\cdots\text{N}_7$ 2.815(4)
	Sb_1-N_2 2.096(4)	$\text{Sb}_1\cdots\text{N}_8$ 2.759(4)
	Sb_1-N_3 2.099(4)	$\text{Sb}_1\cdots\text{N}_9$ 2.779(4)
$\beta-2_2\cdot 3$	Sb_2-N_4 2.086(4)	$\text{Sb}_2\cdots\text{N}_{10}$ 2.751(4)
	Sb_2-N_5 2.077(4)	$\text{Sb}_2\cdots\text{N}_{11}$ 2.886(4)
	Sb_2-N_6 2.089(4)	$\text{Sb}_2\cdots\text{N}_{12}$ 2.864(4)
	Sb_1-N_1 2.078(4)	$\text{Sb}_1\cdots\text{N}_7$ 2.735(4)
	Sb_1-N_2 2.089(4)	$\text{Sb}_1\cdots\text{N}_8$ 2.803(4)
	Sb_1-N_3 2.094(3)	$\text{Sb}_1\cdots\text{N}_9$ 2.822(3)
	Sb_2-N_4 2.101(4)	$\text{Sb}_2\cdots\text{N}_{10}$ 2.733(4)
	Sb_2-N_5 2.081(4)	$\text{Sb}_2\cdots\text{N}_{11}$ 2.768(5)
	Sb_2-N_6 2.090(4)	$\text{Sb}_2\cdots\text{N}_{12}$ 2.865(4)

Optimization of the structure of 2-TPA starting from the crystallographic coordinates reveals a minimum with only two PnBs that is only 8 kJ/mol higher in energy than the initial prediction with three PnBs. Evaluation of the ESP of 2-TPA in the observed solid-state geometry reveals a residual V_{max} of only 53 kJ/mol at the third PnB site. This number is sufficiently low that weak hydrogen bonding can compete and, indeed, a short distance (3.030 Å) is observed between N_7 and the methylene carbon on TPA in the solid-state structure. This marked decrease in the magnitude of the V_{max} suggests negative cooperativity upon formation of the PnBs. This contrasts with systems that use multiple halogens to achieve complementary halogen bonding motifs. Negative cooperativity is not observed in these multitopic systems which

Table 2. DFT Calculated Parameters and AIM Analysis of 2 with PnB Acceptors

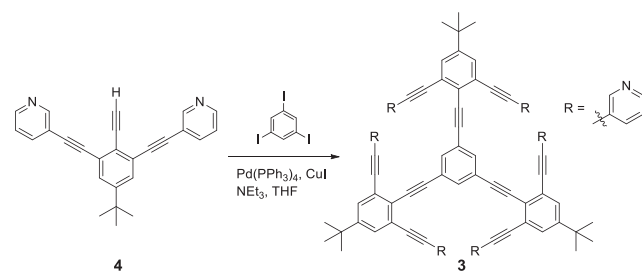
	2·Py	2·Py ₂	2·Py ₃	2·BP ₂ ^c	2·TPA ^a	2·TPA ^b	2 ₂ ·3
Sb—N (Å)	2.105	2.125	2.128	2.098	2.137	2.131	2.127, 2.127
	2.083	2.121	2.128	2.074	2.132	2.107	2.128, 2.127
	2.084	2.093	2.128	2.065	2.136	2.118	2.128, 2.127
Sb···N (Å)	2.703	2.764	2.812	2.637	2.843	2.752	2.799, 2.802
		2.784	2.814	3.197	2.911	2.764	2.798, 2.797
			2.815		2.901	3.438	2.800, 2.796
N—Sb···N (deg)	155.2	154.54	152.49	158.79	166.12	162.1	152.79, 152.46
		154.38	152.39	154.41	172.2	161.7	152.67, 152.46
			152.36		171.39		152.69, 152.83
$\rho_{\text{Sb} \cdots \text{N}}$ (e Å ⁻³)	0.0339	0.0301	0.0274	0.0380	0.0240	0.0307	0.0282, 0.0282
		0.0289	0.0275	0.0128	0.0266	0.0316	0.0282, 0.0280
			0.0276		0.0237	0.0043	0.0282, 0.0283
$\nabla^2 \rho_{\text{Sb} \cdots \text{N}}$ (e Å ⁻⁵)	0.0555	0.0522	0.0506	0.0631	0.0477	0.0530	0.0521, 0.0521
		0.0509	0.0508	0.0299	0.0500	0.0532	0.0521, 0.0519
			0.0508		0.0474	0.0138	0.0519, 0.0522
					0.0393		

^aConformation with four points of attachment (see Figure S6). ^bConformation from the crystal structure (see Figure S6). ^cConformation from the crystal structure with optimized hydrogen positions.

contrasts with the multivalent pnictogen bond donor presented here.^{1,48–50}

In order to circumvent this apparent problem of negative cooperativity, and fully take advantage of the ability of antimony to form three PnBs, a more rigid tridentate PnB acceptor was designed. The design of PnB acceptor 3 exploits the relatively low barrier to rotation of single bonds within diarylacetylene units which can act as hinges for the rigid ditopic pyridyl arms.⁵¹ A similar, but inverted, approach has been used by Huber and co-worker as well, where multitopic halogen bond donors were able to self-assemble with a tripodal halogen bond acceptor.⁴⁸ Threefold Sonogashira coupling of precursor 4 to triiodobenzene yields an arylene ethynylene (AE) system (3) in which coplanarity is impossible due to the overlap of the pyridyl R groups (Scheme 5). Twisted AE

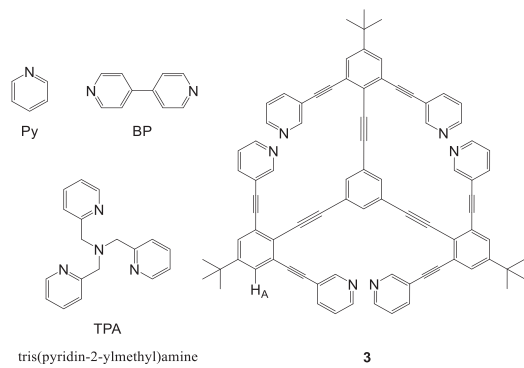
Scheme 5. Generation of 3 via Threefold Coupling



plane in a position to best accommodate a second threefold PnB interaction. It was reasoned that this preorganization would provide positive cooperativity for binding two equivalents of PnB donor, potentially offsetting the apparent negative cooperativity observed for three-fold binding in TPA.

X-ray quality single crystals were grown by treating PnB acceptor 3 with 2 equiv of 2 in benzene. Two polymorphs, α and β , were identified and single crystal analysis revealed that both contained the anticipated ratio of 2 and 3 giving the supramolecular assembly α -2₂·3. The complete assembly from α -2₂·3 is displayed in Figure 4. PnBs hold the two molecules together, and the ethynylpyridine arms are unfolded in a cylindrical conformation with a molecule of 2 capping each of the top and bottom of the cylinder. The ethynylpyridine arms are at approximate right angles (90.03–93.49°) to the central benzene of 3, creating two pockets that are approximately 4 Å in diameter. In the crystal structure, this space is occupied part partially intruding solvent molecules. The second phase, β -2₂·3, is shown in Figure S3 and has the same connectivity as the first. In both phases, numerous solvents of crystallization are observed. All of the PnBs appear to be strong based on the relatively short distances observed in the solid-state structure (Table 1). The Sb···N PnB distances in α -2₂·3 range from 2.751 to 2.886 Å, and the distances in β -2₂·3 range from 2.735 to 2.865 Å. These distances all fall below 80% of Σr_{vdW} or 137% of Σr_{cov} . Analogous to 2·TPA, the Sb—N primary bonds are elongated by 1.73% and 1.28% for the α and β phases,

Scheme 4. Structures of Pyridyl-Based PnB Acceptors



structures can be reinforced via covalent bonds^{52,53} or noncovalent interactions^{54,55} and can be used to introduce cavities in appropriately designed systems.⁵⁶ In this study, it was surmised that PnB could act as a driving force for holding the three ethynylpyridine arms perpendicular to the central benzene ring. Not only does this create a cavity within the supramolecular construct (Figure 4), but also it forces the ethynylpyridine arms on the opposite side of the equatorial

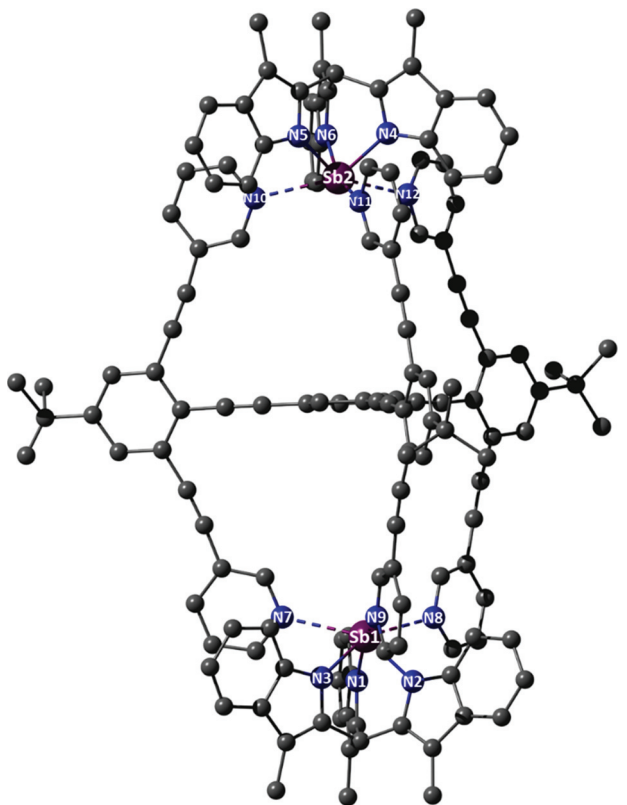


Figure 4. Ball and stick presentation of $\alpha\text{-}2\cdot3$ (hydrogens are omitted for clarity).

respectively. Comparison between the chemical shifts of different protons of **2**, **3**, and $2\cdot3$ confirms self-assembly of $2\cdot3$ in a benzene solution (see Figure S18). The chemical shifts reveal C_3 symmetry, suggesting that the supramolecule is highly symmetrical. A geometry optimization of a model of $2\cdot3$ (lacking *t*-butyl groups) shows that all PnB distances are equal within ± 0.003 Å and the supramolecular structure has a C_3 rotation axis. Furthermore, the electron density at the bond critical points for all the pnictogen bonds are identical within 1% (Table 2). The high symmetry in solution and in the calculated structure suggest that the deviations from this that are observed in the solid state structure of $2\cdot3$ are the result of packing rather than being electronic in origin.

Pnictogen Bond Formation with Monodentate PnB Acceptors. In order to evaluate the role of cooperativity in the formation of multiple PnBs, **2** was treated with monodentate PnB acceptors pyridine (Py) and 4,4'-bipyridine (BP) (Scheme 4). Crystalline $2\cdot1/2\text{C}_6\text{H}_6$ is only partially soluble in nonpolar solvents such as toluene and benzene. Addition of 1–3 equiv of the monodentate PnB acceptors assisted in the dissolution of **2**. Leaving the solutions undisturbed for 24 h resulted in the formation of X-ray quality single crystals. As shown in Figure 5, there are only two PnBs formed between **2** and the monodentate PnB acceptors, Py and BP, in the solid state. For 2-Py_2 , the PnBs between $\text{Sb}\cdots\text{N}_4$ and $\text{Sb}\cdots\text{N}_5$ are both 2.716(6) Å which is 75% of Σr_{vdW} (129% of Σr_{cov}), an indication of strong Pn-bonding. Although there are three PnB donor sites available on the antimony in **2**, a third interaction is not observed. Similar results were observed with BP where the single crystal X-ray structure reveals a 1:1 2:BP stoichiometry. As BP is ditopic, this again results in only two PnBs formed with **2** (Scheme 6). Here, strong and weak interactions are

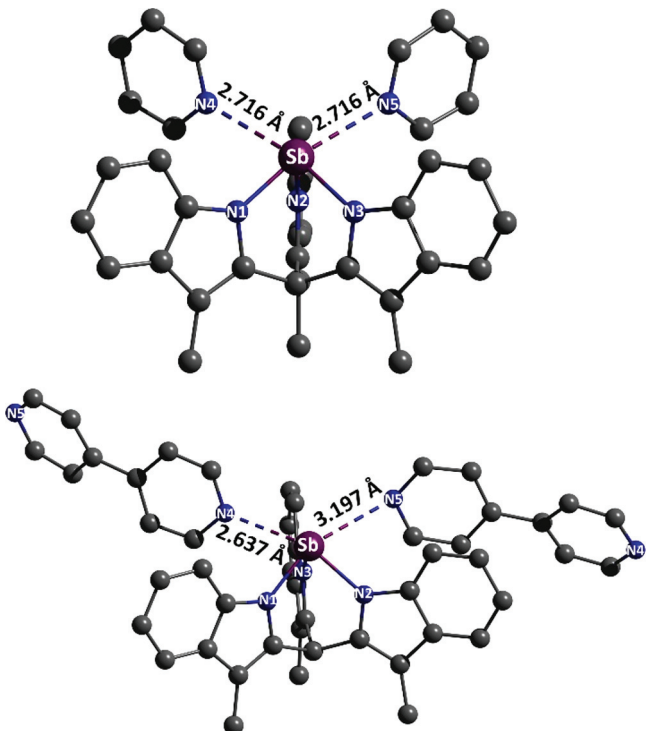
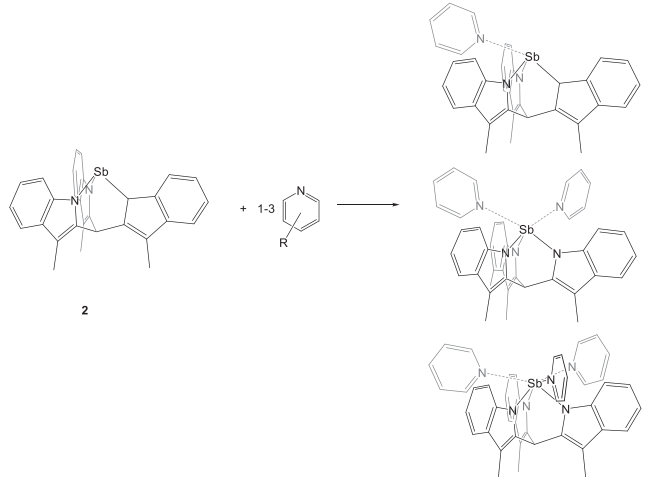


Figure 5. Ball and stick representation of crystal structure of 2-Py_2 (top) and 2-BP (bottom). Hydrogens are omitted for clarity.

Scheme 6. Self-Assembly of Triple PnB Donor **2 with One to Three Pyridine Rings**



observed. The $\text{Sb}\cdots\text{N}_4$ distance is 2.637(2) Å (73% of Σr_{vdW} , 126% of Σr_{cov}) and the $\text{Sb}\cdots\text{N}_5$ distance is 3.197(2) Å (89% of Σr_{vdW} , 152% of Σr_{cov}). Furthermore, there appears to be a suboptimal alignment of the pyridyl ring with the PnB vector. The longer PnB may result from the packing arrangement. Closer inspection of the structure reveals a short $\pi\cdots\pi$ distance between the N_5 pyridine ring and the N_2 indolyl ring ($d_{\text{C}18\cdots\text{C}37} = 3.224$ Å vs $\Sigma r_{\text{vdW}} = 3.4$ Å) that may energetically offset the longer and misaligned PnB. AIM analysis reveals a bcp (0.0128 e Å⁻³) that supports the presence of a weak interaction between the Sb and N atoms (see Table 2). Ultimately, the combination of **2** and BP results in a zigzag polymeric structure assembled through strong and weak PnBs (see Figure S5).

Given the three large V_{\max} values calculated for **2**, it was surprising that only two sites were occupied. DFT calculations were used to probe for evidence of negative cooperativity in sequential PnB formation. Electrostatic potential maps were evaluated for **2**·Py and **2**·Py₂ (Figure 6) to determine the

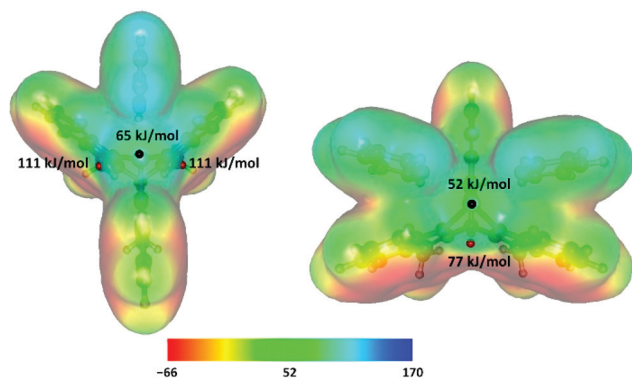


Figure 6. Electrostatic potential of **2**·Py (left) and **2**·Py₂ (right) mapped on the 0.001 au molecular surface (red and black spheres indicated on ESP are V_{\max} and V_{\min} , respectively). ESP units are in kJ/mol.

influence of PnB formation on the magnitude of the remaining V_{\max} sites. Addition of one pyridine molecule to **2** results in a decrease of the remaining V_{\max} values at the antimony to 111 kJ/mol, a decrease of 36 kJ/mol compared with **2**. Addition of the second Py results in a further reduction of the remaining V_{\max} to 77 kJ/mol. In comparison, the V_{\max} value calculated for iodobenzene, which has not been observed to form halogen bonds in the solid state, is 63 kJ/mol. This appears consistent with the apparent inability of **2** to form a third PnB with a monodentate PnB acceptor. An additional point is that, according to the ESP map, the hydrogens on pyridine molecules have V_{\max} values of 119 and 103 kJ/mol for **2**·Py and **2**·Py₂, respectively (cf. 52 kJ/mol Py). This increase in V_{\max} at the pyridine alongside the decrease at the antimony may lead to competition with hydrogen bonding.

The apparent inability to form a third PnB can also be rationalized using an orbital model. The energy of the orbital corresponding to the lone pair on Sb in **2** was plotted as a function of PnB formation with pyridine. Figure 7 depicts a significant increase in energy of this orbital with each subsequent PnB. This suggests an increase in stereochemical activity with each additional Py. This would result in increased repulsion between the PnB donor and the new acceptor, making the formation of the third PnB less favorable. To complement this, the lowest energy Sb–N σ^* orbitals from **2**·Py_n ($n = 0–3$) were extracted from the calculations. In an orbital model, these would be expected to overlap with the occupied lone-pair orbital on the PnB acceptor. As illustrated in Figure 7, the addition of each Py molecule increases the energy of the Sb–N σ^* orbital(s) which causes a reduction in the electrophilicity of **2** toward PnB formation as a result of inefficient energetic overlap with the third Py molecule. To visualize this effect, the Fukui function ($f^*(r)$) integrated from above was mapped onto the molecular surface of **2**·Py and **2**·Py₂ represented by the 0.001 au isosurface of the electron density of each supramolecule (Figure S9). Both color maps are at the same scale, and the results show a great drop in the electrophilicity of **2**·Py₂ compared to **2**·Py. This trend is mirrored by the calculated binding energy for each subsequent

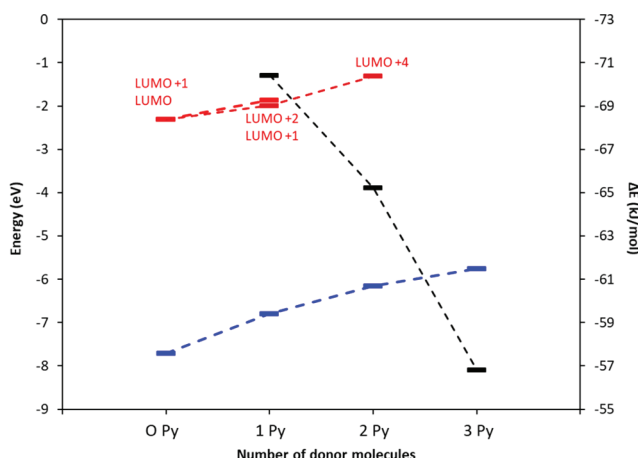


Figure 7. Energy of the low-energy Sb–N σ^* orbitals (red) and 5s orbital on antimony (blue) in **2**·Py_n ($n = 0–3$) and stepwise binding energy (**2**·Py_n + Py → **2**·Py_{n+1}, $n = 0–3$) plotted in black. Dashed lines have been added as a visual aid.

addition of a pyridine plotted in Figure 7. Here, each additional pyridine experiences a nonlinear decrease in stepwise binding energy. Ultimately, the third binding step is 14 kJ/mol less favorable than the first, further evidence of negative cooperativity.

AIM analysis revealed bcp's at the PnBs in each of the supramolecules ($\rho_{\text{Sb}...N}$ in Table 2). A decrease in density with the addition of each subsequent pyridine molecule was observed for **2**·Py_n ($n = 1–3$), consistent with the decrease in PnB strength. The cooperativity enforced by the highly organized pnictogen bond acceptor **3** resulted in bcp's with higher density than the bcp's calculated in **2**·Py₃, implying that the PnBs in **2**·**3** are stronger than the individual added pyridines.

Careful design of a rigid multidentate PnB acceptor is needed to overcome the negative cooperativity associated with multiple PnB formation at an antimony center. Alternatively, strategies to enhance the electrophilicity of the pnictogen could be targeted. These could include modifications to the tripodal support or inclusion of a less electronegative pnictogen.

Pnictogen Bond Formation and Self-Assembly in Solution. To further quantify the PnB donor ability of **2** in solution, binding constants for **2**·Py and **2**·BP were measured by fitting the changes in the UV–vis spectra accompanying a titration. Solutions of **2** in a noncoordinating solvent (DCM) were titrated with each PnB acceptor. Self-assembly was assumed to occur stepwise and the data extracted from the titrations were fit to a 1:1 binding model.³⁶ More complex models were tested but no significant improvement to the fit was observed. The 1:1 binding constants with both pyridine and 4,4'-bipyridine (Table 3) are on the larger side as compared to those observed for neutral halogen-bond donors ($K = 2.3 \times 10^6 \text{ M}^{-1}$ with ICl, 77 M^{-1} with I₂, 0.8 M^{-1} with

Table 3. Binding Constants and $\Delta G_{\text{binding}}$ Determined by UV–Vis Spectroscopy at 293 K

compd	$K (\text{M}^{-1})$	$\Delta G (\text{kJ/mol})$
2 ·Py	1.75×10^4	-23.8
2 ·BP	1.22×10^4	-22.9

$\text{NO}_2\text{C}_6\text{H}_4\text{C}_2\text{I}$,^{57,58} consistent with the large calculated V_{\max} values.

To investigate the solution behavior of the supramolecular cage **2**·**3**, diffusion coefficients of **2**, **3**, and **2**·**3** were measured by pulsed-field gradient spin echo (PFGSE) NMR spectroscopy. Inspection of the crystal structures suggests that **2** should diffuse faster than the much larger supramolecule, and as a result **2**·**3** must have a smaller diffusion coefficient. Fitting the PFGSE NMR signals for the protons on the methyl groups of **2** (labeled as 2-Me) reveals a diffusion coefficient of 5.24×10^{-10} m²/s for **2**. A similar analysis using the *tert*-butyl and H_a (indicated in **Scheme 4**) protons of **3** (labeled as 3-^tBu and 3-H_a) yields smaller diffusion coefficient as compared to **2**, consistent with the larger size of **3**. The same sets of peaks were analyzed in a solution containing **2**·**3** and all the protons in the indicated groups of the supramolecule had both smaller and similar diffusion coefficients than isolated **2** or **3** (**Table 4**).

Table 4. Chemical Shifts (δ), Diffusion Coefficients (D) and Stokes Radii of **2, **3**, and **2**·**3** Studied by PFGSE NMR Spectroscopy of ^1H Nuclei**

compd	δ (ppm)	D (m ² /s)	R_{H} (nm)
2-Me	2.35	5.24×10^{-10}	0.67
3- ^t Bu	1.04	4.67×10^{-10}	0.75
3-H _a	7.64	4.56×10^{-10}	0.77
2 · 3 -(Me)	2.74 ($\Delta\delta = 0.39$)	4.09×10^{-10}	0.86
2 · 3 -(^t Bu)	1.08 ($\Delta\delta = 0.04$)	4.26×10^{-10}	0.82
2 · 3 -(H _a)	7.72 ($\Delta\delta = 0.08$)	4.19×10^{-10}	0.83

Assuming a hard sphere model, the Stokes radii can be calculated from the diffusion coefficients. The size increases as expected from **2** to **3** to **2**·**3**. These measurements are in accord with **2**·**3** remaining intact in solution. In addition to diffusion analysis, difference between the chemical shifts (**Table 4**) of the methyl groups on **2** and **2**·**3** further confirms the integrity of the supramolecule.

The formation of the **2**·**3** assembly and its persistence in solution lends credence to the idea of using the triple pnictogen bonding motif as a new design element for the vertices of supramolecular capsules and cages. The predictable geometric arrangements can potentially be used to self-assemble cavities tailored to guests by incorporating functional groups that can form specific interactions. Given the trend of increasing interaction strength down a group, it can perhaps also be expected that the use of bismuth can lead to stronger pnictogen bonds.

CONCLUSION

In summary, a new antimony-based triple pnictogen bond donor compound, **2**, was prepared and structurally characterized. No pnictogen bonds were observed in crystal structure of **2** by itself. The propensity to form pnictogen bonds was suggested by the large V_{\max} values on the electrostatic surface potential map and confirmed by short pnictogen bonds with pyridyl PnB acceptors. Negative cooperativity was observed with pyridine, bipyridine, and tris(2-pyridylmethyl)amine. DFT calculations revealed a stepwise decrease in the residual V_{\max} values with each sequential pyridine binding. Solution studies suggest a rather high 1:1 binding constant compared with neutral halogen bond donors, highlighting the strength of the pnictogen bonds. Perfect complementarity between the triple PnB donor and an acceptor was achieved by engineering

positive cooperativity into the PnB acceptor. An acetylene hinged, rigid ditopic system was designed that acted as a triple pnictogen bond donor to form a supramolecular assembly with open cavities. Diffusion NMR studies revealed that the supramolecular structure was maintained in solution. The use of a complementary triple pnictogen bond donor/acceptor pairs represents a new strategy for enforcing predictable heteromolecular self-assembly. Furthermore, this structure and its solution stability suggest the use of triple pnictogen bonding as a design element for supramolecular capsule formation.

ASSOCIATED CONTENT

Supporting Information

The Supporting Information is available free of charge on the ACS Publications website at DOI: [10.1021/acs.inorgchem.9b02761](https://doi.org/10.1021/acs.inorgchem.9b02761).

Full synthetic procedures, characterization data, X-ray data analysis, computational methods, UV-vis titration fits, and diffusion NMR fits([PDF](#))
[xyz Coordinates \(ZIP\)](#)

Accession Codes

CCDC 1916107–1916112 contain the supplementary crystallographic data for this paper. These data can be obtained free of charge via www.ccdc.cam.ac.uk/data_request/cif, or by emailing data_request@ccdc.cam.ac.uk, or by contacting The Cambridge Crystallographic Data Centre, 12 Union Road, Cambridge CB2 1EZ, UK; fax: +44 1223 336033.

AUTHOR INFORMATION

Corresponding Authors

*Email: anthony.f.cozzolino@ttu.edu.

*Email: nbowling@uwsp.edu.

ORCID

Shiva Moaven: [0000-0002-9846-2961](http://orcid.org/0000-0002-9846-2961)

Miranda C. Andrews: [0000-0002-6007-404X](http://orcid.org/0000-0002-6007-404X)

Daniel K. Unruh: [0000-0002-2594-5786](http://orcid.org/0000-0002-2594-5786)

Eric Bosch: [0000-0002-6465-1879](http://orcid.org/0000-0002-6465-1879)

Nathan P. Bowling: [0000-0002-6930-1333](http://orcid.org/0000-0002-6930-1333)

Anthony F. Cozzolino: [0000-0002-1100-0829](http://orcid.org/0000-0002-1100-0829)

Author Contributions

The manuscript was written through contributions of all authors. All authors have given approval to the final version of the manuscript.

Notes

The authors declare no competing financial interest.

ACKNOWLEDGMENTS

Research funding (CHE 1847878) and instrument support (NMR: CHE 1048553) from the National Science Foundation are acknowledged by the TTU group. The UWSP and Missouri State groups acknowledge research (CHE 1606558, CHE 1606556) and instrument support (NMR: CHE 0957080, HR-MS: CBET 0958711) from the National Science Foundation.

REFERENCES

- (1) Dumele, O.; Trapp, N.; Diederich, F. Halogen Bonding Molecular Capsules. *Angew. Chem., Int. Ed.* **2015**, *54*, 12339–12344.
- (2) Riwar, L.-J.; Trapp, N.; Root, K.; Zenobi, R.; Diederich, F. Supramolecular Capsules: Strong versus Weak Chalcogen Bonding. *Angew. Chem., Int. Ed.* **2018**, *57* (S2), 17259–17264.

(3) Aakeröy, C. B.; Rajbanshi, A.; Metrangolo, P.; Resnati, G.; Parisi, M. F.; Desper, J.; Pilati, T. The Quest for a Molecular Capsule Assembled via Halogen Bonds. *CrystEngComm* **2012**, *14* (20), 6366–6368.

(4) Starbuck, J.; Norman, N. C.; Orpen, A. G. Secondary Bonding as a Potential Design Element for Crystal Engineering. *New J. Chem.* **1999**, *23*, 969–972.

(5) Metrangolo, P.; Resnati, G. Halogen Bonding: A Paradigm in Supramolecular Chemistry. *Chem. - Eur. J.* **2001**, *7* (12), 2511–2519.

(6) Gleiter, R.; Werz, D. B.; Rausch, B. J. A World beyond Hydrogen Bonds? -Chalcogen-Chalcogen Interactions Yielding Tubular Structures. *Chem. - Eur. J.* **2003**, *9* (12), 2676–2683.

(7) Cavallo, G.; Metrangolo, P.; Pilati, T.; Resnati, G.; Terraneo, G. Naming Interactions from the Electrophilic Site. *Cryst. Growth Des.* **2014**, *14* (6), 2697–2702.

(8) Desiraju, G. R.; Ho, P. S.; Kloo, L.; Legon, A. C.; Marquardt, R.; Metrangolo, P.; Politzer, P.; Resnati, G.; Rissanen, K. Definition of the Halogen Bond (IUPAC Recommendations 2013). *Pure Appl. Chem.* **2013**, *85* (8), 1711–1713.

(9) Politzer, P.; Murray, J. S.; Clark, T. Halogen Bonding: An Electrostatically-Driven Highly Directional Noncovalent Interaction. *Phys. Chem. Chem. Phys.* **2010**, *12* (28), 7748–7757.

(10) Politzer, P.; Murray, J. S.; Clark, T. Halogen Bonding and Other σ -Hole Interactions: A Perspective. *Phys. Chem. Chem. Phys.* **2013**, *15* (27), 11178–11189.

(11) Ke, L.-S.; Myahkostupov, M.; Castellano, F. N.; Gabbaï, F. P. Stibonium Ions for the Fluorescence Turn-On Sensing of F⁻ in Drinking Water at Parts per Million Concentrations. *J. Am. Chem. Soc.* **2012**, *134* (37), 15309–15311.

(12) Hirai, M.; Gabbaï, F. P. Lewis Acidic Stiborafluorenes for the Fluorescence Turn-on Sensing of Fluoride in Drinking Water at Ppm Concentrations. *Chem. Sci.* **2014**, *5* (5), 1886–1893.

(13) Hirai, M.; Gabbaï, F. P. Squeezing Fluoride out of Water with a Neutral Bidentate Antimony(V) Lewis Acid. *Angew. Chem., Int. Ed.* **2015**, *54* (4), 1205–1209.

(14) Christianson, A. M.; Gabbaï, F. P. Anion Sensing with a Lewis Acidic BODIPY-Antimony(V) Derivative. *Chem. Commun.* **2017**, *53* (16), 2471–2474.

(15) Park, G.; Brock, D. J.; Pellois, J.-P.; Gabbaï, F. P. Heavy Pnictogenium Cations as Transmembrane Anion Transporters in Vesicles and Erythrocytes. *Chem.* **2019**, *5* (8), 2215–2227.

(16) Arias Ugarte, R.; Devarajan, D.; Mushinski, R. M.; Hudnall, T. W. Antimony(V) Cations for the Selective Catalytic Transformation of Aldehydes into Symmetric Ethers, α,β -Unsaturated Aldehydes, and 1,3,5-Trioxanes. *Dalton Trans.* **2016**, *45* (27), 11150–11161.

(17) Yang, M.; Gabbaï, F. P. Synthesis and Properties of Triarylhalostibonium Cations. *Inorg. Chem.* **2017**, *56* (15), 8644–8650.

(18) Chitnis, S. S.; Sparkes, H. A.; Annibale, V. T.; Pridmore, N. E.; Oliver, A. M.; Manners, I. Addition of a Cyclophosphine to Nitriles: An Inorganic Click Reaction Featuring Protio, Organo, and Main-Group Catalysis. *Angew. Chem., Int. Ed.* **2017**, *56* (32), 9536–9540.

(19) Yang, M.; Tofan, D.; Chen, C.-H.; Jack, K. M.; Gabbaï, F. P. Digging the Sigma-Hole of Organoantimony Lewis Acids by Oxidation. *Angew. Chem., Int. Ed.* **2018**, *57* (42), 13868–13872.

(20) Tolman, C. A. Steric Effects of Phosphorus Ligands in Organometallic Chemistry and Homogeneous Catalysis. *Chem. Rev.* **1977**, *77* (3), 313–348.

(21) Xu, Y.; Huang, J.; Gabidullin, B.; Bryce, D. L. A Rare Example of a Phosphine as a Halogen Bond Acceptor. *Chem. Commun.* **2018**, *54* (78), 11041–11043.

(22) Lisac, K.; Topić, F.; Arhangelskis, M.; Cepić, S.; Julien, P. A.; Nickels, C. W.; Morris, A. J.; Friščić, T.; Cincić, D. Halogen-Bonded Cocrystallization with Phosphorus, Arsenic and Antimony Acceptors. *Nat. Commun.* **2019**, *10* (1), 61.

(23) Benz, S.; Poblador-Bahamonde, A. I.; Low-Ders, N.; Matile, S. Catalysis with Pnictogen, Chalcogen, and Halogen Bonds. *Angew. Chem., Int. Ed.* **2018**, *57* (19), 5408–5412.

(24) Moaven, S.; Yu, J.; Yasin, J.; Unruh, D. K.; Cozzolino, A. F. Precise Steric Control over 2D versus 3D Self-Assembly of Antimony(III) Alkoxide Cages through Strong Secondary Bonding Interactions. *Inorg. Chem.* **2017**, *56* (14), 8372–8380.

(25) Hough, E.; Nicholson, D. G.; Vasudevan, A. K. Stereochemical Role of Lone Pairs in Main-Group Elements. Part 3. Structure and Bonding in Trichloro(1,4,7,10,13-Pentaoxacyclopentadecane)-Antimony(III) Studied by Means of X-Ray Crystallography at 120 K. *J. Chem. Soc., Dalton Trans.* **1987**, No. 2, 427–430.

(26) Alcock, N. W.; Ravindran, M.; Roe, S. M.; Willey, G. R. Synthesis and Structure of Antimony(III)Chloride-1,4,7,10,13,16-Hexaoxacyclooctadecane-(18-Crown-6)-Acetonitrile (1/1/1). *Inorg. Chim. Acta* **1990**, *167* (1), 115–118.

(27) Schäfer, M.; Pebler, J.; Dehnicke, K. Synthese, Kristallstrukturen und ^{121}Sb -Mößbauer-Spektren von $[\text{SbBr}_3(15\text{-Krone-5})]$, $[\text{SbBr}_2\text{Me}(15\text{-Krone-5})]$ und $[\text{SbBr}_2\text{Ph}(15\text{-Krone-5})]$. *Z. Anorg. Allg. Chem.* **1992**, *611* (5), 149–157.

(28) Pohl, S.; Haase, D.; Peters, M. Kristall- und Molekülstruktur von $\text{SbI}_3 \cdot 9\text{S}_3$ ($9\text{S}_3 = 1,4,7\text{-Trithiacyclonan}$). *Z. Anorg. Allg. Chem.* **1993**, *619* (4), 727–730.

(29) Farina, P.; Levason, W.; Reid, G. Synthesis and Structures of Antimony(III) Halide Complexes with Oxa-Thia and Oxa-Selena Crowns. *Polyhedron* **2013**, *55*, 102–108.

(30) Moaven, S.; Yu, J.; Vega, M.; Unruh, D. K.; Cozzolino, A. F. Self-Assembled Reversed Bilayers Directed by Pnictogen Bonding to Form Vesicles in Solution. *Chem. Commun.* **2018**, *54* (64), 8849–8852.

(31) Leroy, C.; Johannson, R.; Bryce, D. L. 121/123Sb Nuclear Quadrupole Resonance Spectroscopy: Characterization of Non-Covalent Pnictogen Bonds and NQR Crystallography. *J. Phys. Chem. A* **2019**, *123*, 1030.

(32) Mokrai, R.; Barrett, J.; Apperley, D. C.; Batsanov, A. S.; Benkő, Z.; Heift, D. Weak Pnictogen Bond with Bismuth: Experimental Evidence Based on Bi-P Through-Space Coupling. *Chem. - Eur. J.* **2019**, *25* (16), 4017–4024.

(33) Burschka, Ch. Intermolekulare Koordination Bei Zyklischen Estern Der Stibonigen Und Der Thiostibonigen Säure. *Z. Anorg. Allg. Chem.* **1978**, *446* (1), 185–192.

(34) Ensinger, U.; Schwarz, W.; Schrutz, B.; Sommer, K.; Schmidt, A. Methoxostibane. Struktur Und Schwingungsspektren. *Z. Anorg. Allg. Chem.* **1987**, *544* (1), 181–191.

(35) Aguilà, D.; Escribano, E.; Speed, S.; Talancón, D.; Yermán, L.; Alvarez, S. Calibrating the Coordination Chemistry Tool Chest: Metrics of Bi- and Tridentate Ligands. *Dalton Trans.* **2009**, *2009* (33), 6610–6625.

(36) Loya, J. D.; Qiu, J.; Unruh, D. K.; Cozzolino, A. F.; Hutchins, K. M. Co-Crystallization of the Anti-Cholesterol Drug Bezafibrate: Molecular Recognition of a Pharmaceutical Contaminant in the Solid State and Solution via Hydrogen Bonding. *Cryst. Growth Des.* **2018**, *18* (9), 4838–4843.

(37) Aakeröy, C. B.; Chopade, P. D.; Desper, J. Establishing a Hierarchy of Halogen Bonding by Engineering Crystals without Disorder. *Cryst. Growth Des.* **2013**, *13* (9), 4145–4150.

(38) Aakeröy, C. B.; Fasulo, M.; Schultheiss, N.; Desper, J.; Moore, C. Structural Competition between Hydrogen Bonds and Halogen Bonds. *J. Am. Chem. Soc.* **2007**, *129* (45), 13772–13773.

(39) Krueger, E. L.; Sinha, A. S.; Desper, J.; Aakeröy, C. B. Exploring Binding Preferences in Co-Crystals of Conformationally Flexible Multitopic Ligands. *CrystEngComm* **2017**, *19* (31), 4605–4614.

(40) Lohrman, J. A.; Deng, C.-L.; Shear, T. A.; Zakharov, L. N.; Haley, M. M.; Johnson, D. W. Methanesulfonyl-Polarized Halogen Bonding Enables Strong Halide Recognition in an Arylethynyl Anion Receptor. *Chem. Commun.* **2019**, *55* (13), 1919–1922.

(41) Garrett, G. E.; Gibson, G. L.; Straus, R. N.; Seferos, D. S.; Taylor, M. S. Chalcogen Bonding in Solution: Interactions of Benzotelluradiazoles with Anionic and Uncharged Lewis Bases. *J. Am. Chem. Soc.* **2015**, *137* (12), 4126–4133.

(42) von Dobeneck, H.; Prietzel, H. Weitere Beobachtungen Zur Reaktion Zwischen Aldehyden Und Indolderivaten (III. Mitteil. Zur

Chemie Des Indols). *Hoppe-Seyler's Z. Für Physiol. Chem.* **1955**, 299 (1), 214–226.

(43) Schmidbaur, H.; Nowak, R.; Huber, B.; Mueller, G. Hexaethylbenzene-Trichloroantimony: A Menshutkin Complex with a Centroid Antimony-Arene Coordination. *Organometallics* **1987**, 6 (10), 2266–2267.

(44) Mootz, D.; Händler, V. Crystal Structure of the Menshutkin Complex Benzene · 2SbCl₃. *Z. Anorg. Allg. Chem.* **1986**, 533 (2), 23–29.

(45) Cangelosi, V. M.; Pitt, M. A.; Vickaryous, W. J.; Allen, C. A.; Zakharov, L. N.; Johnson, D. W. Design Considerations for the Group 15 Elements: The Pnictogen- π Interaction As a Complementary Component in Supramolecular Assembly Design. *Cryst. Growth Des.* **2010**, 10 (8), 3531–3536.

(46) Mantina, M.; Chamberlin, A. C.; Valero, R.; Cramer, C. J.; Truhlar, D. G. Consistent van Der Waals Radii for the Whole Main Group. *J. Phys. Chem. A* **2009**, 113 (19), 5806–5812.

(47) Cordero, B.; Gómez, V.; Platero-Prats, A. E.; Revés, M.; Echeverría, J.; Cremades, E.; Barragán, F.; Alvarez, S. Covalent Radii Revisited. *Dalton Trans.* **2008**, 0 (21), 2832–2838.

(48) Jungbauer, S. H.; Bulfield, D.; Kniep, F.; Lehmann, C. W.; Herdtweck, E.; Huber, S. M. Toward Molecular Recognition: Three-Point Halogen Bonding in the Solid State and in Solution. *J. Am. Chem. Soc.* **2014**, 136 (48), 16740–16743.

(49) Turunen, L.; Beyeh, N. K.; Pan, F.; Valkonen, A.; Rissanen, K. Tetraiodoethynyl Resorcinarene Cavitands as Multivalent Halogen Bond Donors. *Chem. Commun.* **2014**, 50 (100), 15920–15923.

(50) Lieffrig, J.; Jeannin, O.; Fourmigué, M. Expanded Halogen-Bonded Anion Organic Networks with Star-Shaped Iodoethynyl-Substituted Molecules: From Corrugated 2D Hexagonal Lattices to Pyrite-Type 2-Fold Interpenetrated Cubic Lattices. *J. Am. Chem. Soc.* **2013**, 135 (16), 6200–6210.

(51) Toyota, S. Rotational Isomerism Involving Acetylene Carbon. *Chem. Rev.* **2010**, 110 (9), 5398–5424.

(52) Menning, S.; Krämer, M.; Coombs, B. A.; Rominger, F.; Beeby, A.; Dreuw, A.; Bunz, U. H. F. Twisted Tethered Tolanes: Unanticipated Long-Lived Phosphorescence at 77 K. *J. Am. Chem. Soc.* **2013**, 135 (6), 2160–2163.

(53) Iwaniuk, D. P.; Wolf, C. A Stereodynamic Probe Providing a Chiroptical Response to Substrate-Controlled Induction of an Axially Chiral Arylacetylene Framework. *J. Am. Chem. Soc.* **2011**, 133 (8), 2414–2417.

(54) Nandy, R.; Subramoni, M.; Varghese, B.; Sankararaman, S. Intramolecular π -Stacking Interaction in a Rigid Molecular Hinge Substituted with 1-(Pyrenylethynyl) Units. *J. Org. Chem.* **2007**, 72 (3), 938–944.

(55) Sharber, S. A.; Baral, R. N.; Frausto, F.; Haas, T. E.; Müller, P.; Thomas III, S. W. Substituent Effects That Control Conjugated Oligomer Conformation through Non-Covalent Interactions. *J. Am. Chem. Soc.* **2017**, 139 (14), 5164–5174.

(56) Hirata, O.; Takeuchi, M.; Shinkai, S. Allosteric Binding of Anionic Guests to a Bicyclic Host Which Imitates the Action of a 'Turnstile'. *Chem. Commun.* **2005**, No. 30, 3805–3807.

(57) Beale, T. M.; Chudzinski, M. G.; Sarwar, M. G.; Taylor, M. S. Halogen Bonding in Solution: Thermodynamics and Applications. *Chem. Soc. Rev.* **2013**, 42 (4), 1667–1680.

(58) Dumele, O.; Wu, D.; Trapp, N.; Goroff, N.; Diederich, F. Halogen Bonding of (Iodoethynyl)Benzene Derivatives in Solution. *Org. Lett.* **2014**, 16 (18), 4722–4725.